Osteoarthritis and Cartilage xxx (2018) 1–11

Osteoarthritis and Cartilage

OARSI OSTEOARTHRITIS RESEARCH SOCIETY INTERNATIONAL

Cartilage-on-cartilage contact: effect of compressive loading on tissue deformations and structural integrity of bovine articular cartilage

L. Zevenbergen † *, W. Gsell ‡, L. Cai §, D.D. Chan ||, N. Famaey ¶, J. Vander Sloten ¶, U. Himmelreich ‡, C.P. Neu § #, I. Jonkers †

† *Human Movement Biomechanics Research Group, Department of Movement Sciences, KU Leuven, Leuven, Belgium*
‡ *Biomedical MRI, Department of Imaging and Pathology, KU Leuven, Leuven, Belgium*
§ *Weldon School of Biomedical Engineering, Purdue University, West Lafayette, IN, USA*
|| *Department of Biomedical Engineering, Rensselaer Polytechnic Institute, Troy, NY, USA*
¶ *Biomechanics Section, Department of Mechanical Engineering, KU Leuven, Leuven, Belgium*
# *Department of Mechanical Engineering, University of Colorado Boulder, Colorado, USA*

ARTICLE INFO

Article history:
Received 17 October 2017
Accepted 21 August 2018

Keywords:
Articular cartilage
DENSE
Compressive loading
Displacements
Strain
MRI relaxometry

SUMMARY

Objective: This study aims to characterize the deformations in articular cartilage under compressive loading and link these to changes in the extracellular matrix constituents described by magnetic resonance imaging (MRI) relaxation times in an experimental model mimicking *in vivo* cartilage-on-cartilage contact.

Design: Quantitative MRI images, T_1, T_2 and $T_{1\rho}$ relaxation times, were acquired at 9.4T from bovine femoral osteochondral explants before and immediately after loading. Two-dimensional intra-tissue displacement and strain fields under cyclic compressive loading (350N) were measured using the displacement encoding with stimulated echoes (DENSE) method. Changes in relaxation times in response to loading were evaluated against the deformation fields.

Results: Deformation fields showed consistent patterns among all specimens, with maximal strains at the articular surface that decrease with tissue depth. Axial and transverse strains were maximal around the center of the contact region, whereas shear strains were minimal around the contact center but increased towards contact edges. A decrease in T_2 and $T_{1\rho}$ was observed immediately after loading whereas the opposite was observed for T_1. No correlations between cartilage deformation patterns and changes in relaxation times were observed.

Conclusions: Displacement encoding combined with relaxometry by MRI can noninvasively monitor the cartilage biomechanical and biochemical properties associated with loading. The deformation fields reveal complex patterns reflecting the depth-dependent mechanical properties, but intra-tissue deformation under compressive loading does not correlate with structural and compositional changes. The compacting effect of cyclic compression on the cartilage tissue was revealed by the change in relaxation time immediately after loading.

Introduction

In vivo assessment of the mechanical behavior of articular cartilage-on-cartilage contact under compressive loading could provide insights into cartilage mechanics in healthy and diseased joints. In osteoarthritis, with disease progression, the mechanical properties of the tissue change, affect the cellular response and contribute to matrix damage. Therefore, non-invasive monitoring of intra-tissue deformation could serve as a unique biomarker for tissue damage and disease progression.

* Address correspondence and reprint requests to: L. Zevenbergen, Department of Movement Sciences, KU Leuven, Tervuursevest 101 – bus 1501. BE 3001 Leuven, Belgium. Tel: 32-16-37-94-63.

E-mail addresses: lianne.zevenbergen@kuleuven.be (L. Zevenbergen), willy.gsell@kuleuven.be (W. Gsell), cai101@purdue.edu (L. Cai), chand5@rpi.edu (D.D. Chan), nele.famaey@kuleuven.be (N. Famaey), jos.vandersloten@kuleuven.be (J. Vander Sloten), uwe.himmelreich@kuleuven.be (U. Himmelreich), cpneu@colorado.edu (C.P. Neu), ilse.jonkers@kuleuven.be (I. Jonkers).

https://doi.org/10.1016/j.joca.2018.08.009

Articular cartilage is an anisotropic and inhomogeneous material with depth-dependent mechanical properties due to variation in composition and structure of the extracellular matrix. The depth-wise variation in collagen orientation and concentration controls the tensile and dynamic compressive stiffness of articular cartilage[1,2]. Likewise, the depth-wise variation in proteoglycan concentration creates local variation in osmotic pressure and swelling and is therefore primarily responsible for the static compressive stiffness[2,3]. Increased water content will decrease the aggregate compressive modulus of cartilage[4].

Depth-dependent mechanical behavior of articular cartilage is often evaluated using optical imaging techniques, such as tracking of fluorescently labeled cells[5–7] or image pattern tracking with digital imaging correlation[8–11]. However, these techniques are invasive and require cutting the tissue through its thickness, to expose the surface to be imaged. Consequently, the mechanical response during loading is inherently hampered by the loss of cartilage integrity and can therefore not easily be translated to clinical applications.

To measure load-induced displacements, defined as the difference between the final and initial point in the tissue throughout the cartilage thickness, magnetic resonance imaging (MRI) by tag registration[12,13] or displacement encoding with stimulated echoes (DENSE)[14–18] have been used. Displacement encoding with stimulated echoes (DENSE) MRI allows measuring intra-tissue displacements from a fixed encoding time using the phase signal[15,19]. Previous DENSE studies with cartilage explants were performed with indenters[14], which are significantly stiffer than cartilage tissue. Therefore, cartilage-on-cartilage contact would be more realistic in mimicking the synovial joint, and thus more relevant when studying cartilage pathology *in vivo*.

Furthermore, quantitative MRI relaxometry, relates to the structure and composition of the cartilage matrix[17]. The depth-wise anisotropic T_2 signal has been linked to orientation changes in the collagen network[20,21] and water content[22]. $T_{1\rho}$ strongly correlates with changes in proteoglycan content[23,24] and T_1 with the water content[22,25].

It is intuitive to expect external loading of articular cartilage to change the orientation of the collagen fibers, the concentration of proteoglycans, and water shifts, which consequently may affect the relaxation times. Several studies have documented a decrease of T_1[26,27], T_2[28–30], and $T_{1\rho}$[29,30] under applied loading. However, it is less clear if these changes relate to the loading-induced mechanical deformations and if they persist after loading.

The goals of this study are two-fold. First, we describe displacement and strain patterns of cartilage-on-cartilage contact in explants under cyclic compressive loading emulating *in vivo* condition in a synovial joint. Second, the load-induced deformation fields were related to local changes in the structure and concentration of the cartilage constituents as reflected in T_1, T_2 and $T_{1\rho}$. We hypothesized that compressive loading would decrease T_1, T_2 and $T_{1\rho}$, especially in the contact regions that experience high strains, due to matrix compaction and water extrusion.

Methods

Sample preparation

Eight stifle joints from 9-month-old bovines were obtained from a slaughterhouse within 1 day of slaughtering. The selection of this age range was motivated by the comparable thickness of the bovine cartilage to human cartilage and its good health[31]. Osteochondral explants with 30 mm diameter were harvested from the load-bearing area of medial and lateral femoral condyles. The subchondral bone layer of the explants was potted using bone cement (VersoCit2, Struers, Denmark) for fixation in the sample holder. After preparation, the explants were immersed in phosphate buffered saline (PBS) and stored at 8°C for maximally 5 days.

Applied loading

A custom built loading apparatus was designed, similar to Chan *et al.*, 2009[15], to cyclically compress the two paired osteochondral explants within a MRI system [Fig. 1(A)]. A double-acting pneumatic cylinder applied 350N compressive load (representing ≈0.33 times body weight) to the explants during 2.0 s constant loading followed by 1.4 s unloading [Fig. 1(B)], inducing an average contact stress of 2.78 ± 1.47 MPa, representative for moderate activities of daily living in humans[32]. The explants were aligned with opposing surfaces perpendicular to the loading direction; the lateral explant served as the indenting explant and the medial explant was fixed. To prevent dehydration and susceptibility artefacts at the cartilage interface during imaging, the explants were submerged in degassed PBS (sonicated for 30 min).

Before DENSE image acquisition, the osteochondral explants were cyclically loaded for ≈500 cycles [Fig. 1(B)–(C)]. This resulted in a steady state load-deformation response, with standard deviation of the displacements below half the spatial resolution (58.6 μm) of the MRI image[12,15].

MRI acquisition

All MRI data were acquired on a horizontal 9.4 T MRI system (BioSpec 94/20USR, Bruker Medical GMBH, Ettlingen, Germany) using a quadrature birdcage coil with a 72 mm internal diameter.

First, a high-resolution 2D T_2-weighted RARE anatomical reference scan was acquired. Before and immediately after the loading protocol, quantitative relaxation time measurements were collected for a single image slice through the center of the cartilage explants [Fig. 1(A)]. T_1 mapping was conducted using a variable repetition time (TR) of 220, 350, 500, 1000, 2000, and 4000 ms with RARE readout (RARE-VTR). T_2 was assessed through multi-echo spin echo sequence with echo time (TE) of 11.5, 23, 34.5, 46, 57.5, 69, 80.5, and 92 ms. The spin-lock durations (TSL) of the $T_{1\rho}$ sequence were 10, 20, 40, 60, 80, 100, 120, 140, 160, and 180 ms.

A DENSE sequence measured the orthogonal cartilage displacements during compressive loading (≈1200 cycles). Two data sets with a displacement-encoding gradient area of 2.55 π/mm in the *x*-direction and 1.92 π/mm in the *y*-direction were acquired. A reference scan, without displacement-encoding gradient, was also acquired to eliminate displacement-independent phase contributions. Each scan used four phase cycled repetitions for cosine and sine modulation (CANSEL) to eliminate the anti-echo and T_1 decay artifacts[33], and 40 averages to improve the SNR. For image readout, a steady-state free precession (SSFP) sequence was used. An overview of all acquisition parameters and scan durations can be found in supplementary table S1.

Image reconstruction and data analysis

Both opposing cartilage layers were manually segmented in the DENSE and relaxation images using the polygon selection tool in ImageJ[34]. Pixel-by-pixel maps of the relaxation time constants were determined to the equations below using a Levenberg–Marquardt mono-exponential curve-fitting algorithm[35] in Python 3.4.1 (Python Software Foundation, https://www.python.org/):

$$S(TR) = S_0(1 - exp(-TR/T_1))$$

Please cite this article in press as: Zevenbergen L, et al., Cartilage-on-cartilage contact: effect of compressive loading on tissue deformations and structural integrity of bovine articular cartilage, Osteoarthritis and Cartilage (2018), https://doi.org/10.1016/j.joca.2018.08.009

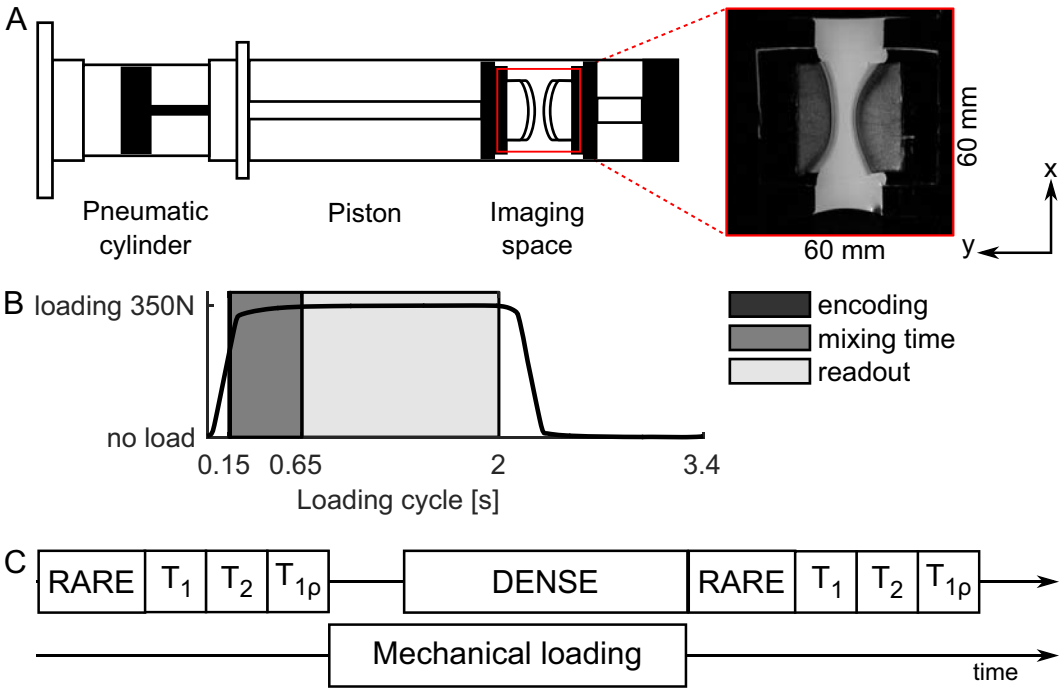

Fig. 1. A) Schematic diagram of the loading apparatus and imaging space. B) The loading profile was gated with the protocol for the displacement encoding with stimulated echoes (DENSE) imaging to ensure precise timing; the encoding gradient was applied prior to loading at 0.15 s. After the mixing period (0.15–0.65 s), the displacement images were acquired during the loaded phase (0.65–2 s). C) Quantitative imaging protocol; anatomical scan (RARE), relaxation measures (T_1, T_2, $T_{1\rho}$) and displacement encoding with stimulated echoes (DENSE) during compressive loading: ≈500 cycles of pre-loading were applied followed by ≈1200 cycles during DENSE imaging.

$$S(TE) = S_0 exp(-TE/T_2)$$

$$S(TSL) = S_0 exp(-TSL/T_{1\rho})$$

where S is the image signal at a given time point $-TR$ for T_1 maps, $-TE$ for T_2 maps or $-TSL$ for $T_{1\rho}$ maps, and S_0 the initial magnetization. Variation in T_2 throughout the cartilage depth was analyzed to verify maturation[36].

The DENSE raw data were processed off-line using MATLAB (2015a, The Mathworks, Natick, MA). The phase-modulated data were recombined using CANSEL[33] to isolate the displacement-encoded echo, before applying a two-dimensional inverse Fourier transform. Subsequently, first-order phase correction of the opposing cartilage layers was performed on the reference scan and applied to the displacement-encoded images. Next, the corrected phases were unwrapped using a region-growing algorithm[37] with manual correction of pixels which presented ±2π difference with its neighbors. Phase differences between the reference scan and the displacement-encoded scans were converted into transverse (dX) and axial displacement (dY). Displacements were smoothed using a two-dimensional robust locally weighted linear regression method, with matrix size of 256. Strains were then computed using a maximum likelihood estimation of the deformation gradient tensor[38]. Green-Lagrange strain data were reported as transverse (E_{xx}) and axial components (E_{yy}), with the corresponding shear strain (E_{xy}).

Cartilage thickness was computed perpendicular to the segmented articular surface. Each surface was divided in seven sub-regions of equal width as function of the transverse location with five zones describing the contact area (CA1 – CA5) and two adjacent zones without contact (NC1 & NC2) (Fig. 2). In view of the limited spatial resolution, three parallel cartilage layers of equal thickness (2–4 pixels per layer) were identified throughout the cartilage depth based on the cartilage masks; superficial zone (SZ), middle zone (MZ), and deep zone (DZ). In each subdivision, displacements, strains and relaxation measures were averaged to compare regional trends between explants across the transverse location and tissue depth.

To evaluate deformation, the average cartilage thickness profile across the contact area before and after loading was compared using a paired samples t-test.

To analyze the cartilage deformation parameters (dX, dY, E_{xx}, E_{yy}, E_{xy}), a repeated measures linear mixed-effects (LME) model with explant (medial/lateral), transverse location (NC1, CA1-CA5, NC2), tissue depth (SZ, MZ and DZ), and their interactions as fixed effects, with medial explant, the central contact region (CA3) and DZ as reference categories and using subjects as grouping variable. The model was fitted using maximum likelihood estimation. The

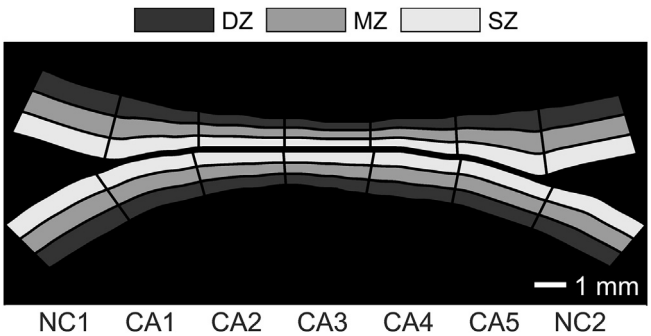

Fig. 2. Locations of the cartilage sub-regions used for statistical analysis of displacement and strain distributions in both explants (medial – top, lateral – bottom of the image). Comparisons were made at three tissue depths; deep zone (DZ), middle zone (MZ) and superficial zone (SZ) and at different transverse locations; two zones without contact (NC1, NC2) and five zones that describe the contacting area (CA1-CA5).

Please cite this article in press as: Zevenbergen L, et al., Cartilage-on-cartilage contact: effect of compressive loading on tissue deformations and structural integrity of bovine articular cartilage, Osteoarthritis and Cartilage (2018), https://doi.org/10.1016/j.joca.2018.08.009

interaction terms were only retained when the full model did show significant interactions. The coefficients of the regression model were reported as significantly different from zero at 5% significance levels.

Similarly, differences in relaxation times (ΔT_1, ΔT_2, and $\Delta T_{1\rho}$) before and after loading, with respect to depth, transverse location, and explant, were compared. To account for individual differences, between subject variation was modeled as a random effect.

To evaluate the association between the change in cartilage composition and structure immediately after loading and the tissue deformation during compressive loading a two-tailed Pearson's linear correlation test was used. For all three tissue depths, the strain fields were correlated to the difference in relaxation times before and after loading, including the average values for each transverse location to account for the measurement noise. Given clustering of the data, the assumption of independence has been violated and no *P*-value can be reported.

All statistical processing was performed with MATLAB (2015a, The Mathworks, Natick, MA).

Results

The average contact region between the two indenting explants was 13.45 ± 2.48 mm, applying an average contact stresses of 2.78 ± 1.47 MPa (assuming a circular contact area). After loading, the average cartilage thickness decreased significantly from 1.77 ± 0.35 mm to 1.67 ± 0.31 mm ($P = 0.003$) (Fig. 3).

Figure 4 represents displacements (A), strains (B) and relaxation times before (C) and immediately after loading (D) in a representative sample.

The average axial displacement was maximal (83.65 ± 35.75 μm) at the middle of the cartilage–cartilage contact region and decreased significantly towards the edges of the contact region (CA1, CA5) and non-contacting regions [Fig. 5(D)–(F)]. The transverse displacements left from the central contact region (CA2) were significantly lower compared to the central contact region whereas the regions to the right (CA4, CA5 and NC2) were significantly higher [Fig. 5(A)–(C)]. Tissue in the non-contacting region was deformed as well, especially in the transverse direction. Displacements in axial and transverse direction were significantly higher in the SZ compared to the DZ. The transverse displacements in the lateral explants were significantly higher compared to the medial explant, while the opposite was observed for axial displacements (Fig. 5(C) and (F)).

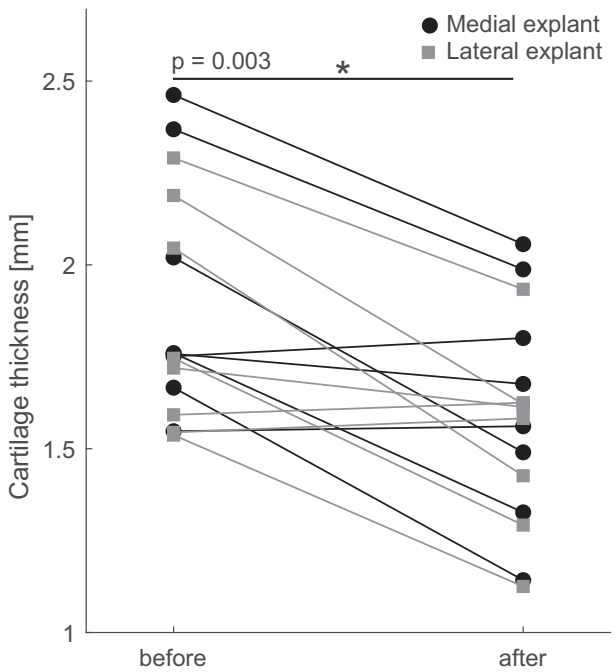

Fig. 3. Average cartilage thickness throughout the contact region before and immediately after loading.

For the transverse displacements, two-way interactions were found for location and layer, explant and location, and explant and layer. The axial displacements main effects presented an interaction between layer and location. These interaction effects are described in supplementary fig. S1.

The magnitudes of axial (E_{yy}), transverse (E_{xx}) and shear (E_{xy}) strains displayed depth and location varying distribution [Figs. 4(B) and 6]. Overall, the magnitude of the tensile transverse and compressive axial strains were highest at the center of the cartilage–cartilage contact region and decreasing towards the contact edges. Regions without contact and CA1 region presented significantly lower transverse and axial strains compared to the middle contact region [Fig. 6(C) and (F)]. Highest shear were found between the center of the contact region and non-contacting areas, where the strains were lowest. Only CA2 and NC1 present a decrease in shear strains compared to the contact center [Fig. 6(I)]. The strains decreased with depth from the articular surface. However, only the axial and transverse strains were significantly higher in the SZ compared to the DZ. The shear strain in the lateral cartilage explant was significantly lower compared to the medial explant [Fig. 6(I)]. No significant difference between both explants was observed for the transverse and axial strains.

The main effects of the transverse strains were subjected to interactions between location and layer and explant and location. Shear strains presented negative interaction between explant and transverse location. No interaction effects for compressive strains were observed. The interaction effects for transverse and shear strain are presented in supplementary fig. S2.

Immediately after loading, the T_2 and $T_{1\rho}$ decreased, whereas the T_1 increased [Figs. 4(C and D) and 7]. The decrease in T_2 and $T_{1\rho}$ was significantly higher for the MZ and SZ compared to the DZ. The T_1 of the SZ was significantly less increased in the SZ compared to the DZ [Fig. 7(A)–(C)]. The absolute change in $T_{1\rho}$ and T_1 were higher for the non-contacting areas compared to the central contact region, however only significant for one side [Fig. 6(C) and (I)]. For the other locations and T_2 no significant changes were observed [Fig. 7(F)]. The lateral explant presented significantly lower absolute change in $T_{1\rho}$ and T_1. The main effects of all changes in relaxation times were subjected to significant interaction effects between explant and tissue depth (supplementary fig. S4).

The intercept term, reflecting the between subject variation was significantly different from zero, in all deformation and relaxometry linear mixed models, indicating variability between samples (supplementary Fig. S1, Fig. S2, Fig. S4). five explants showed variation in T_2 indicative of a five layer structure, the remaining three showed a seven layer structure (supplementary fig. S3(B)).

At group level, strains presented no correlations with the observed changes in relaxation times, independent of tissue depth. A complete overview of the correlations terms between relaxation parameters and strains is presented in Table I.

Discussion

The objectives of this study were to evaluate the displacements and strains of intact bovine articular cartilage under physiological loading conditions and to evaluate their effect on cartilage structure

Please cite this article in press as: Zevenbergen L, et al., Cartilage-on-cartilage contact: effect of compressive loading on tissue deformations and structural integrity of bovine articular cartilage, Osteoarthritis and Cartilage (2018), https://doi.org/10.1016/j.joca.2018.08.009

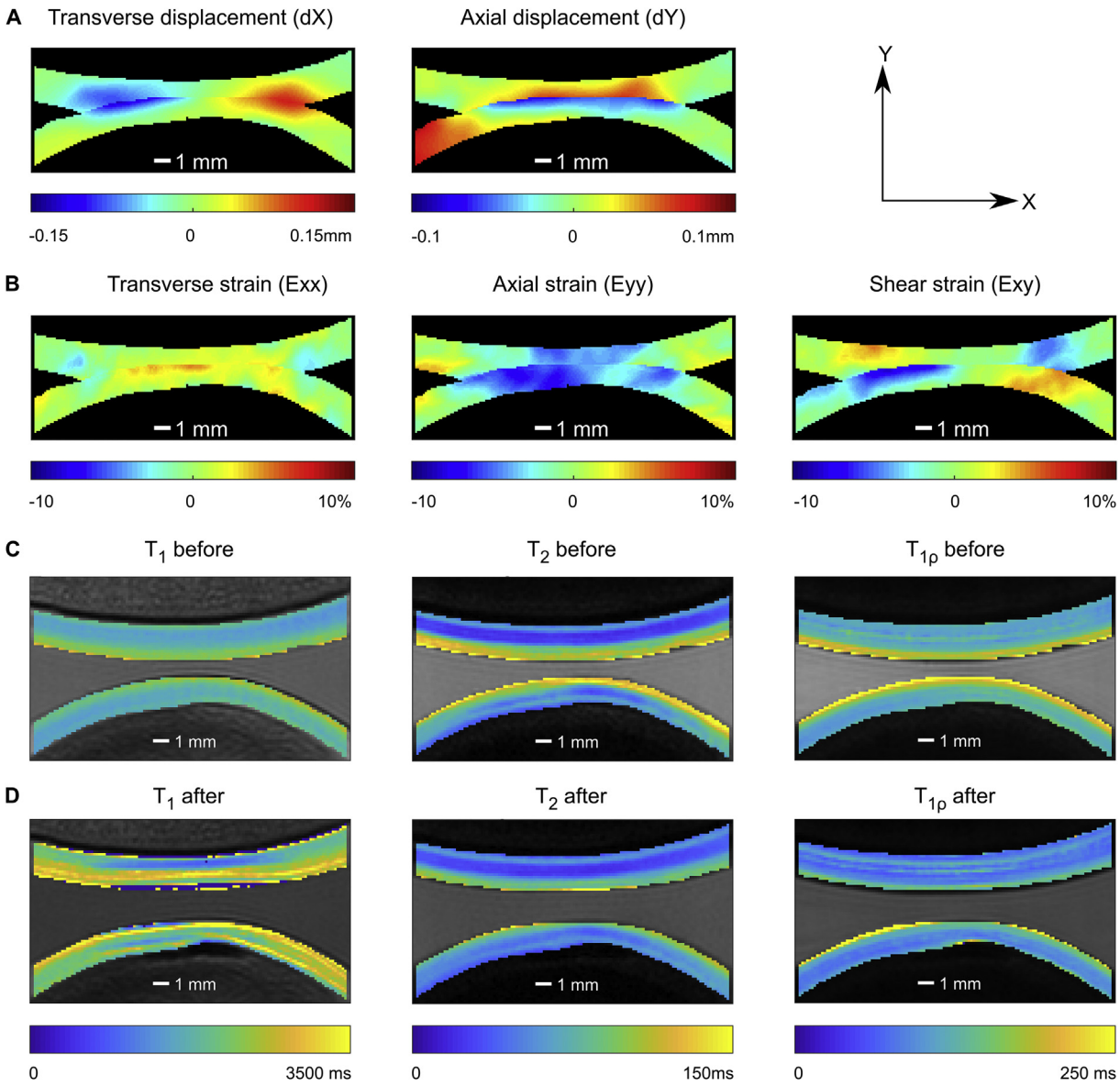

Fig. 4. Two-dimensional displacement (A), strain (B) and T_1, T_2 and $T_{1\rho}$ relaxometry data before (C) and after loading (D) within the articular cartilage layers of a representative sample. The displacements and strains were determined by DENSE during cyclic compressive loading along the Y-axis. The top cartilage layer represents the medial osteochondral explant (static) and the opposing layer the lateral explant (indenting). The T_1, T_2 and $T_{1\rho}$ relaxometry maps were acquired before and immediately after loading using variable repetition time (*TR*), echo time (*TE*) and spin-lock durations (*TSL*), respectively.

and composition through displacement-encoded MRI synchronized with compressive loading and quantitative MRI relaxometry (T_1, T_2 and $T_{1\rho}$). This approach allows to maintain tissue integrity under unconfined compression and to study extended cartilage-on-cartilage contact region.

In agreement with studies in bovine[10,11] and human[18], heterogeneous displacement and strain fields throughout the cartilage were observed, with axial and shear strains being larger than the transverse strain. This can be explained by the higher tangential tensile modulus of articular cartilage compared to its axial compressive modulus[39]. These findings seems to contradict other studies that report minimal shear strains compared to the axial and transverse strains by evaluating one line of interest at the middle of the contact[6,14,16]. In this study, we observed similar results at the contact center. However, evaluating a broader region of interest, the importance of shear strain during compressive loading becomes evident.

Within the contact zone of approximately 13.45 mm, maximal axial and minimal transverse displacements were observed around the center. Moving towards the edges, axial displacements decreased but transverse displacements increased. Consequently, axial and transverse strains were compressive and tensile, respectively, in the contact region with their maximum around the contact center, showing the expected Poisson effect. As a result, the shear strains were near zero around the center of the contact region but increasing towards the edges of the contact zone. These findings agree with the observed strains in the human patellofemoral joint[9] during cartilage-on-cartilage contact where tissue integrity was sacrificed and the *in vivo* results of a tibiofemoral joint[15,18].

The largest gradient in shear strain was observed at the edges of the contact region, indicative of expansion away from the center of pressure. This confirms that not only tissue in the contact region but also adjacent tissue plays an important role in redistributing

Please cite this article in press as: Zevenbergen L, et al., Cartilage-on-cartilage contact: effect of compressive loading on tissue deformations and structural integrity of bovine articular cartilage, Osteoarthritis and Cartilage (2018), https://doi.org/10.1016/j.joca.2018.08.009

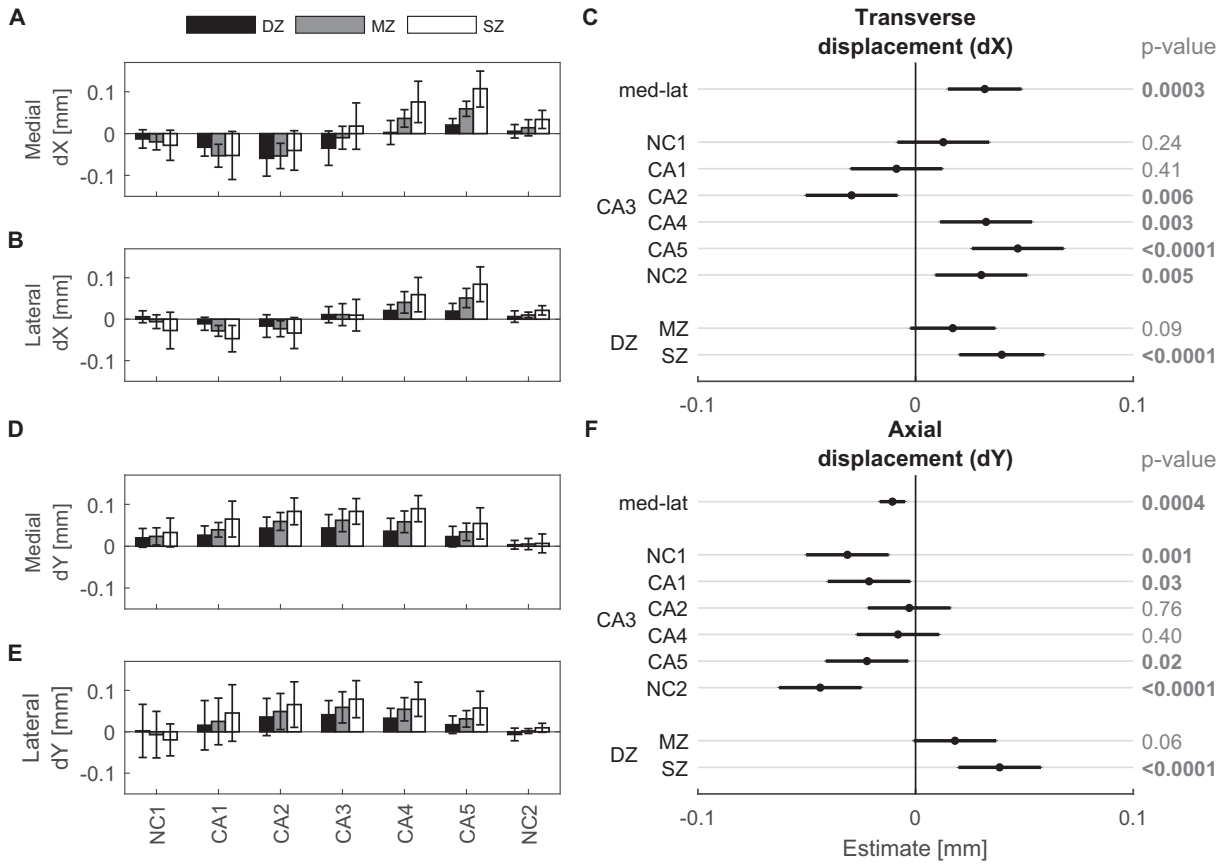

Fig. 5. Transverse (dX) and axial displacements (dY) at selected regions of interest in the medial (A&D) and lateral cartilage layers (B&E). Displacements were calculated at different tissue depths (DZ = deep zone, MZ = middle zone, SZ = superficial zone) for different transverse locations (NC1, NC2 = non-contacting areas, CA1 − CA5 = contact zone) (Fig. 3). Data are expressed as mean ± standard deviations, $n = 8$. Pane C and F represent the linear mixed effect model estimates describing the spatial distribution of the transverse and axial displacements. The horizontal lines represent the 95% confidence intervals for the main parameter estimates, the corresponding *P*-values are given on the right vertical axis. Each model included tissue depth (DZ, MZ, SZ), transverse location (NC1, CA1-CA5, NC2) and explant (med-lat) as fixed effects and subjects as a random effect. The medial explant, central contact region (CA3) and DZ served as reference categories. A negative estimate value indicates that the compared parameter is lower than the reference parameter. The interaction effects and intercept for the described models are presented in supplementary material figure S1.

the applied loads. The transverse displacements and shear strains indicate lateral expansion of the tissue shearing away from the contact point, even towards the non-contacting areas. Especially the superficial tissue bulges towards the zone without contact inducing significantly higher displacements and strains in this zone compared to the DZ. The circular shape of the non-congruent femoral condyles in the absence of surrounding tissue (in particular the menisci), may over-emphasize this effect. However, it mimics the *in vivo* situation more than experiments where cartilage is indented using an indenter with different mechanical properties than native cartilage. The location-dependency of the strain fields under unconfined compressive loading emphasizes the importance of larger explants or *in vivo* whole-joint analysis.

A significant depth-dependent variation in compressive axial and shear, but not transverse tensile strain was found. The maximal compressive strain in axial direction is located at the articular surface and decreases significantly towards the cartilage-subchondral bone interface. This corresponds with previous studies in young[8,10] and adult[13] bovine articular cartilage and reflects the increased compressive modulus of cartilage with distance from the articular surface[5,7,10].

In contrast, minimal increase in transverse tensile strains from the DZ towards the SZ were found. This effect can be related to a depth-dependent decrease in intrinsic tensile modulus from the articular surface[40]. This property is mainly controlled by the depth-wise variation in collagen fibril orientation. Our results therefore suggest that the orientation of the collagen network is optimized such that the cartilage has a greater uniformity in tensile strains parallel to the articular surface through the thickness of the articular cartilage layer. Similar findings in immature and mature cartilage have been observed[8,9,13,15].

Comparable with axial compressive strain, elevated shear strains were found in the SZ decreasing towards the DZ. This is in contrast with studies on mature articular cartilage[8,9,13] that reported the opposite shear strain distribution. Our results are however in agreement with observed shear strain distribution in 6-week-old immature bovine cartilage[8]. Therefore, the relative immaturity of the bovine explants (9 months) in our study needs to be taken into account when interpreting the cartilage behavior, as discussed below.

Relaxation times were measured before and immediately after loading to investigate the effect of loading history on collagen concentration and orientation (T_2), proteoglycan content ($T_{1\rho}$) and water content (T_1 and T_2). Our study presented a decrease in T_2 and $T_{1\rho}$ relaxation time throughout the cartilage depth immediately after loading, conform to previous studies[26,28,30] but in conflict with Nebelung *et al.*, 2017[27]. The conflicting results between studies may be attributable to differences in study design (e.g., *in vitro/in vivo*), specimen selection, age, loading regimen, imaging protocol, and segmentation approach.

Please cite this article in press as: Zevenbergen L, et al., Cartilage-on-cartilage contact: effect of compressive loading on tissue deformations and structural integrity of bovine articular cartilage, Osteoarthritis and Cartilage (2018), https://doi.org/10.1016/j.joca.2018.08.009

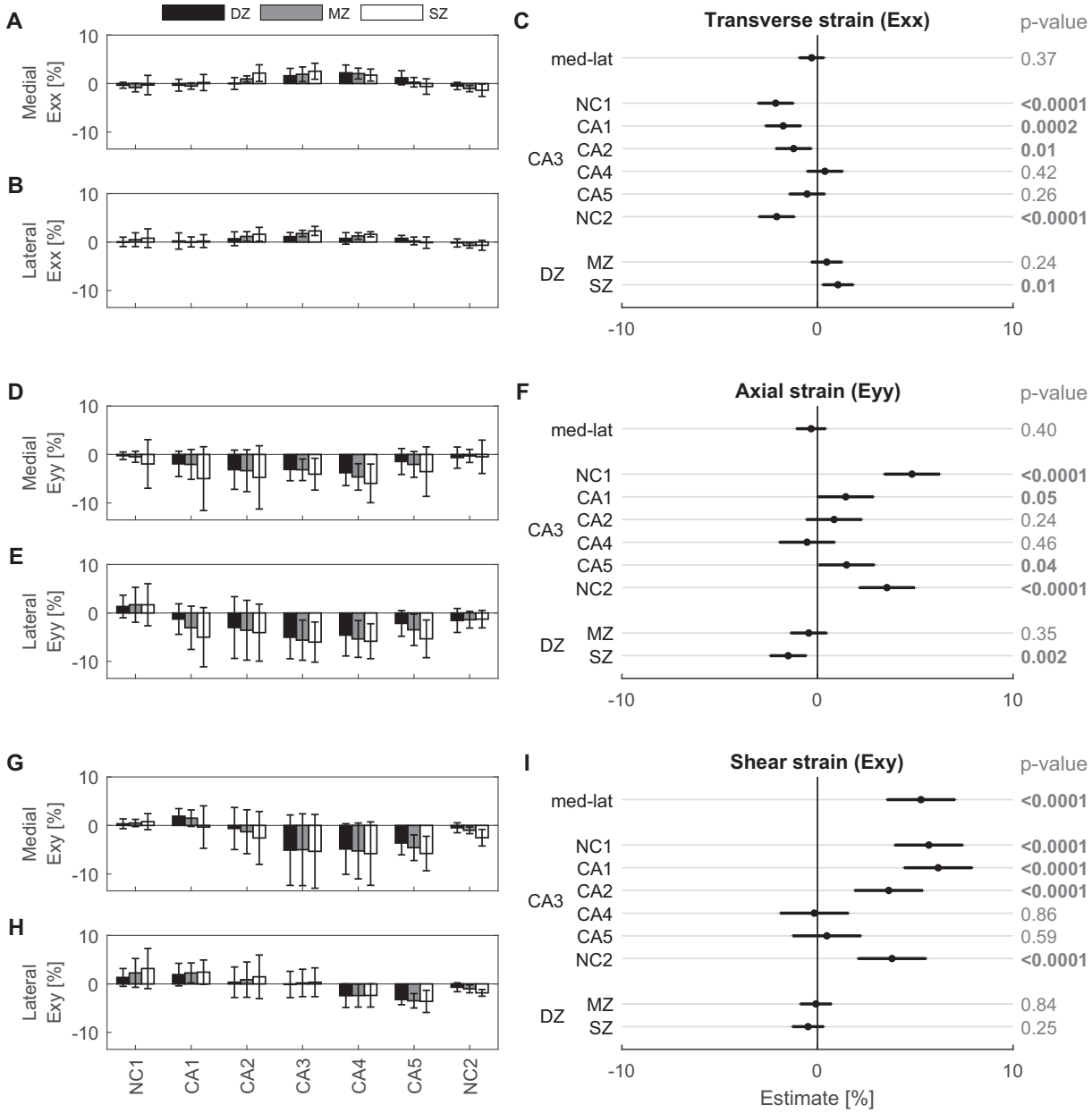

Fig. 6. Green–Lagrange strains; transverse (E_{xx}), axial (E_{yy}) and shear (E_{xy}) at selected regions of interest in the medial (A, D&G) and lateral cartilage layers (B, E&H). Strains were calculated at different tissue depths (DZ = deep zone, MZ = middle zone, SZ = superficial zone) for different transverse locations (NC1, NC2 = non-contacting areas, CA1 – CA5 = contact zone) (Fig. 3). Data are expressed as mean ± standard deviations, $n = 8$. Pane C, F and I represent the linear mixed effect model estimates describing the spatial distribution of the transverse, axial and shear strains. The horizontal lines represent the 95% confidence intervals for the main parameter estimates, the corresponding *P*-values are given on the right vertical axis. Each model included tissue depth (DZ, MZ, SZ), transverse location (NC1, CA1-CA5, NC2) and explant (med-lat) as fixed effects and subjects as a random effect. The medial explant, central contact region (CA3) and DZ served as reference categories. A negative estimate value indicates that the compared parameter is lower than the reference parameter. The interaction effects and intercept for the described models are presented in supplementary material figure S2.

Immediately after the loading, we observed a significant change in cartilage thickness, which suggests compaction of the solid matrix. Additionally, during the different loading cycles (≈1700 repetitions) the interstitial water content could be redistributed within the matrix or extruded to the surrounding fluid. Indeed, the decrease in T_2 reflected the extrusion of water content[22] and altered orientation of the collagen fibrils[20,21], especially in the SZ. The reduction of $T_{1\rho}$ suggests a relative increase in proteoglycan concentration[23,24] as the cartilage volume was reduced due to the loading protocol and water was extruded from the cartilage, rather than an actual increase in proteoglycan concentration. Contra indicative for these findings is the increased T_1 after loading, which positively correlates with the water content[25]. This suggests that water concentration was increased within the tissue, especially in the DZ of the medial explant [Fig. 7(A) and (C)]. This suggests that following loading, part of the interstitial water content was moved to the DZ instead of being extruded from the cartilage surface given the differences in permeability throughout cartilage depth[41]. The increased T_1 in the superficial and MZ might be due to partial recovery of the cartilage after the applied loading[42], although conflicting with previous observations under compressive loading[26,27].

In this study, we found differences in MRI relaxation measures and deformation patterns between the medial and lateral explant under similar loading conditions. These differences could be

Please cite this article in press as: Zevenbergen L, et al., Cartilage-on-cartilage contact: effect of compressive loading on tissue deformations and structural integrity of bovine articular cartilage, Osteoarthritis and Cartilage (2018), https://doi.org/10.1016/j.joca.2018.08.009

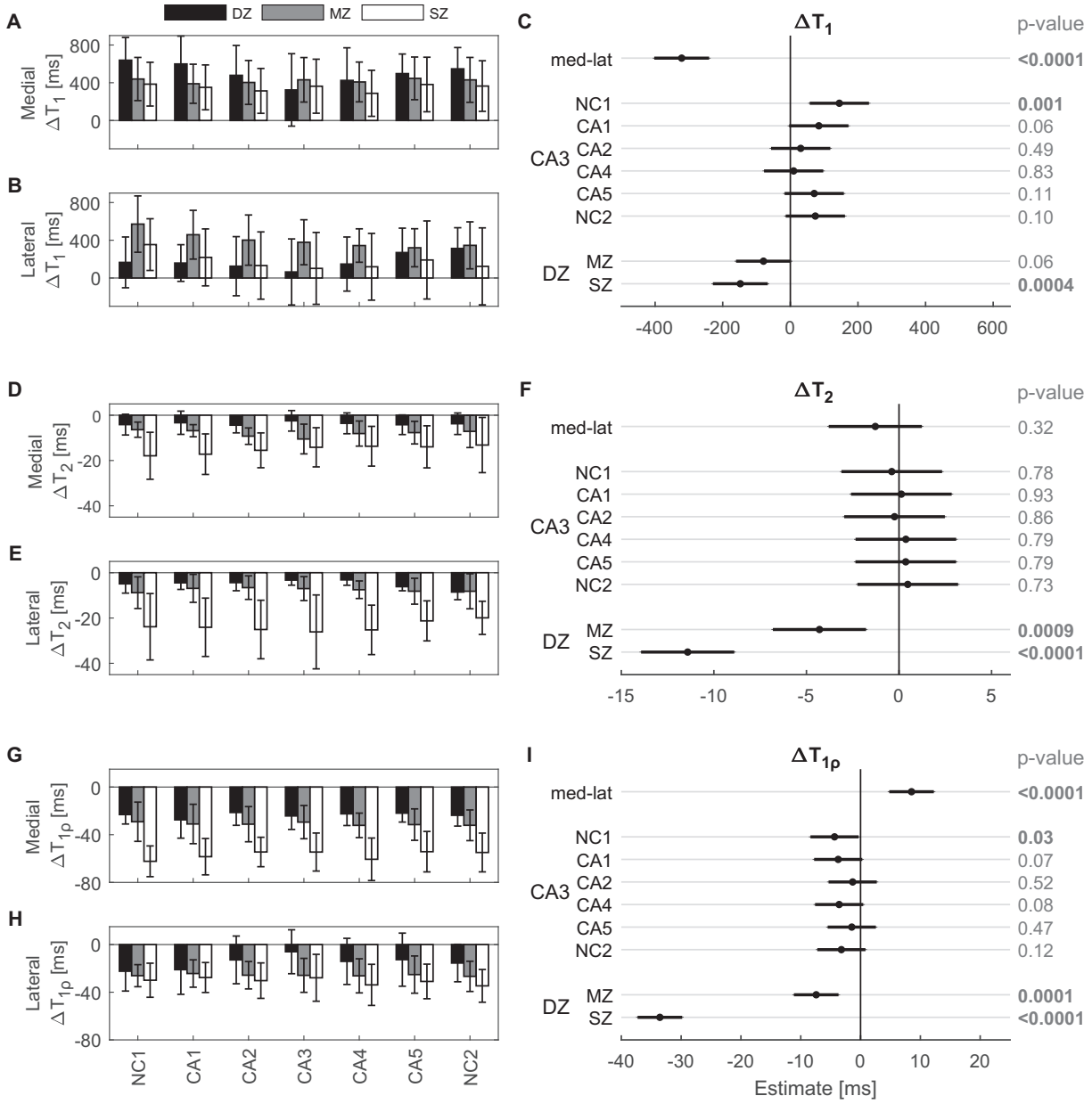

Fig. 7. Difference in cartilage T_1, T_2 and $T_{1\rho}$ relaxation times (immediately after − before loading) at selected regions of interest in the medial (A, D&G) and lateral explant (B, E&H). Relaxation parameters were calculated at different tissue depths (DZ = deep zone, MZ = middle zone, SZ = superficial zone) for different transverse locations (NC1, NC2 = non-contacting areas, CA1 − CA5 = contact zone) (Fig. 3). Data are expressed as mean ± standard deviations, $n = 8$. Pane C, F and I represent linear mixed effect model estimates describing the spatial distribution the relaxation time difference (ΔT_1, ΔT_2 & $\Delta T_{1\rho}$). The horizontal lines represent the 95% confidence intervals for the main parameter estimates, the corresponding *P*-values are given on the right vertical axis. Each model included tissue depth (DZ, MZ, SZ), transverse location (NC1, CA1-CA5, NC2) and explant (med-lat) as fixed effects and subjects as a random effect. The medial explant, central contact region (CA3) and DZ served as reference categories. A negative estimate value indicates that the compared parameter is lower than the reference parameter. The interaction effects and intercept for the described models are presented in supplementary material fig. S4.

Table I
Pearson's linear correlation coefficients between the average changes in relaxation time ($\Delta \boldsymbol{T}_1$, $\Delta \boldsymbol{T}_2$ and $\Delta \boldsymbol{T}_{1\rho}$) at the three different tissue depths (deep zone (DZ), middle zone (MZ), superficial zone (SZ)) before and immediately after loading and the respective average strains ($\boldsymbol{E_{xx}}$, $\boldsymbol{E_{yy}}$, $\boldsymbol{E_{xy}}$). Data from all explants at different regions of interest are pooled together ($n = 80$). None of the correlations were statistically significant

	ΔT_1			ΔT_2			$\Delta T_{1\rho}$		
	DZ	MZ	SZ	DZ	MZ	SZ	DZ	MZ	SZ
E_{xx}	0.02	−0.10	−0.09	0.12	−0.11	−0.02	0.10	0.06	−0.05
E_{yy}	0.07	0.03	0.08	0.13	−0.16	0.15	−0.06	−0.09	−0.00
E_{xy}	0.21	−0.18	−0.15	0.22	0.03	0.20	0.11	0.14	−0.10

attributed to the anatomical variation in composition and mechanical properties among various regions in the knee joint[43]. However, we have to take into account that during the deformation measurements the lateral explant was indenting towards the medial explant. During this movement, it might be that the explant was slightly tilted due to the impact. Since no movement artefacts were observed in the DENSE images, the movement was consistent during the loading and did not jeopardize the displacement results. Nonetheless, this effect may explain some of the described interaction effects for the deformation parameters, most clearly observed in the shear strains, and contribute to the observed variability across samples.

Please cite this article in press as: Zevenbergen L, et al., Cartilage-on-cartilage contact: effect of compressive loading on tissue deformations and structural integrity of bovine articular cartilage, Osteoarthritis and Cartilage (2018), https://doi.org/10.1016/j.joca.2018.08.009

Finally, this study is the first to relate the strain patterns under compressive loading to the spatially varying changes in T_1, T_2 and $T_{1\rho}$ immediately after loading. Unexpectedly, although the strain patterns and relaxation times changed after loading, for none of the three tissue layers correlations were found. This finding seems to suggest that despite the large tissue deformations occurring, immediately following loading the tissue recovers towards a new equilibrium state that is not directly related to the deformations observed during compressive loading. Recently, Linka *et al*., 2017[44] reported correlations between T_2 differences and the matrix constituents and fiber orientations calculated using a computational model during static compressive loading. In contrast, our data shows that difference in relaxometry data before and immediately after loading cannot be used as a surrogate of cartilage mechanics during cyclic compressive loading.

A first confounding factor explaining the variability in deformation patterns as well as relaxometry measures is the age of the animals used in this study. Although the animals did not reach full skeletal maturity at 9 months[45], most of them presented similar structural organization as shown by the variation in T_2 throughout depth (Fig. S3)[36]. The development of the collagen architecture, formation of pyridinoline crosslinks and local changes in proteoglycan distribution during maturation increased the tensile and compressive modulli[46,47] and affect the MR relaxation times[48]. Therefore, the mechanical response of developing articular cartilage under similar loading would result in higher strains compared to skeletal matured tissue. Furthermore, it could be hypothesized that the lack of a fully calcified cartilage layer in the immature tissue will limit the anchorage of the cartilage to the subchondral bone, reducing the shear strains in the DZ. On the other hand, the division of the cartilage depth in three equal zones may obscure depth-specific variation. To better describe this variation, increased spatial resolution of the MRI images is needed.

A second set of confounding factors contributing to the variability across samples, relates to the MRI protocol. The orientation and shape of the articular surface with respect to the applied magnetic field could add to the spatial variability in relaxation times across samples, especially T_2[49]. However, this influence is expected to be minimal as the orientation of the explants before and after loading was similar, and the curvature of the explants was small[49]. Additionally, the role of temperature effects resulting from thermal exchange during magnetization needs to be further elucidated. A temperature change will alter relaxometry measures as documented in water and agarose constructs[50]. The phenomena may therefore obscure the local changes due to loading and induce more overall change in relaxometry parameters, as observed in this study especially in T_1. To date temperature effects in articular cartilage are not documented.

In conclusion, we demonstrated here that displacement encoded imaging combined with relaxometry (T_1, T_2 and $T_{1\rho}$) can noninvasively monitor the cartilage biomechanical properties and biomarkers indicative of biochemical content over time. As such early symptoms of cartilage degeneration could already be associated with changes in cartilage mechanics and constitution prior to morphological signs at joint level. This would allow earlier and targeted treatment. The deformation fields reveal complex deformation patterns reflecting the depth-dependent mechanical properties under cartilage-on-cartilage compressive loading. The effect of cyclic compressive loading on the compaction of the cartilage tissue is reflected in the change in relaxation time immediately after loading. This unique experimental model could be used to study cartilage pathology (e.g., defects, osteoarthritis), in a controlled environment. Furthermore, the results of this study could be used to validate computational models that calculate tissue deformation.

Author contributions

Zevenbergen, Gsell, vander Sloten, Himmelreich and Jonkers contributed to the conception and design of this work. Zevenbergen, Gsell and Jonkers collected the data. Zevenbergen, Cai, Chan, Famaey, Neu, and Jonkers contributed to analysis and interpretation of the data. Zevenbergen takes responsibility for the experimental design, the integrity of the data, and the accuracy of the data analysis. All authors were involved in drafting the article or revising it critically for important intellectual content, and granted final approval of the manuscript.

Conflict of interest

The authors have declared no conflicts of interest.

Role of the funding source

None of the funding sources a have a role in the study design, collection, analysis and interpretation of data, nor in the writing of the manuscript and the decision to submit the manuscript for publication.

Acknowledgements

This research was supported in part by a Ph.D. grant of the Agency for Innovation by Science and Technology (IWT) 131105, the KU Leuven research council OT13083 and IMIR PF10/0117, HERCULES AKUL/13/29 and NIH R01 AR063712 and R21 AR064178. The authors thank Tom Dresselears for technical assistance during data acquisition and Kristof Goavearts for using his software.

Supplementary data

Supplementary data related to this article can be found at https://doi.org/10.1016/j.joca.2018.08.009.

References

1. Bader DL, Kempson GE, Egan J, Gilbey W, Barrett AJ. The effects of selective matrix degradation on the short-term compressive properties of adult human articular cartilage. Biochim Biophys Acta 1992;1116:147–54, https://doi.org/10.1016/0304-4165(92)90111-7.
2. Laasanen MS, Töyräs J, Korhonen RK, Rieppo J, Saarakkala S, Nieminen MT, *et al*. Biomechanical properties of knee articular cartilage. Biorheology 2003;40:133–40.
3. Mow VC, Ratcliffe A, Robin Poole A. Cartilage and diarthrodial joints as paradigms for hierarchical materials and structures. Biomaterials 1992;13:67–97, https://doi.org/10.1016/0142-9612(92)90001-5.
4. Cohen NP, Foster RJ, Mow VC. Composition and dynamics of articular cartilage: structure, function, and maintaining healthy state. J Orthop Sports Phys Ther 1998;28:203–15, https://doi.org/10.2519/jospt.1998.28.4.203.
5. Schinagl RM, Gurskis D, Chen AC, Sah RL. Depth-dependent confined compression modulus of full-thickness bovine articular cartilage. J Orthop Res 1997;15:499–506, https://doi.org/10.1002/jor.1100150404.
6. Wong BL, Bae WC, Chun J, Gratz KR, Lotz M, Sah RL. Biomechanics of cartilage articulation: effects of lubrication and degeneration on shear deformation. Arthritis Rheum 2008;58:2065–74, https://doi.org/10.1002/art.23548.
7. Wong BL, Sah RL. Mechanical asymmetry during articulation of tibial and femoral cartilages: local and overall compressive and shear deformation and properties. J Biomech 2010;43:1689–95, https://doi.org/10.1016/j.jbiomech.2010.02.035.

8. Canal CE, Hung CT, Ateshian GA. Two-dimensional strain fields on the cross-section of the bovine humeral head under contact loading. J Biomech 2008;41:3145–51, https://doi.org/10.1016/j.jbiomech.2008.08.031.
9. Guterl Canal C, Gardner TR, Rajan V, Ahmad CS, Hung CT, Ateshian GA. Two-dimensional strain fields on the cross-section of the human patellofemoral joint under physiological loading. J Biomech 2009;42:1275–81, https://doi.org/10.1016/j.jbiomech.2009.03.034.
10. Wang CCB, Deng J-M, Ateshian GA, Hung CT. An automated approach for direct measurement of two-dimensional strain distributions within articular cartilage under unconfined compression. J Biomech Eng 2002;124:557–67, https://doi.org/10.1115/1.1503795.
11. Wang CCB, Chahine NO, Hung CT, Ateshian GA. Optical determination of anisotropic material properties of bovine articular cartilage in compression. J Biomech 2003;36:339–53, https://doi.org/10.1016/S0021-9290(02)00417-7.
12. Neu CP, Hull ML. Toward an MRI-based method to measure non-uniform cartilage deformation: an MRI-cyclic loading apparatus system and steady-state cyclic displacement of articular cartilage under compressive loading. J Biomech Eng 2003;125:180–8, https://doi.org/10.1115/1.1560141.
13. Neu CP, Hull ML, Walton JH. Heterogeneous three-dimensional strain fields during unconfined cyclic compression in bovine articular cartilage explants. J Orthop Res 2005;23:1390–8, https://doi.org/10.1016/j.orthres.2005.03.022.
14. Neu CP, Walton JH. Displacement encoding for the measurement of cartilage deformation. Magn Reson Med 2008;59:149–55, https://doi.org/10.1002/mrm.21464.
15. Chan DD, Neu CP, Hull ML. Articular cartilage deformation determined in an intact tibiofemoral joint by displacement-encoded imaging. Magn Reson Med 2009;61:989–93, https://doi.org/10.1002/mrm.21927.
16. Chan DD, Neu CP, Hull ML. In situ deformation of cartilage in cyclically loaded tibiofemoral joints by displacement-encoded MRI. Osteoarthritis Cartilage 2009;17:1461–8, https://doi.org/10.1016/j.joca.2009.04.021.
17. Chan DD, Neu CP. Probing articular cartilage damage and disease by quantitative magnetic resonance imaging. J R Soc Interface 2013;10, https://doi.org/10.1098/rsif.2012.0608. 20120608.
18. Chan DD, Cai L, Butz KD, Trippel SB, Nauman EA, Neu CP. In vivo articular cartilage deformation: noninvasive quantification of intratissue strain during joint contact in the human knee. Sci Rep 2016;6:19220, https://doi.org/10.1038/srep19220.
19. Aletras AH, Ding S, Balaban RS, Wen H. DENSE: displacement encoding with stimulated echoes in cardiac functional MRI. J Magn Reson 1999;137:247–52, https://doi.org/10.1006/jmre.1998.1676.
20. Nieminen MT, Rieppo J, Töyräs J, Hakumäki JM, Silvennoinen J, Hyttinen MM, *et al*. T2 relaxation reveals spatial collagen architecture in articular cartilage: a comparative quantitative MRI and polarized light microscopic study. Magn Reson Med 2001;46:487–93, https://doi.org/10.1002/mrm.1218.
21. Xia Y, Moody JB, Burton-Wurster N, Lust G. Quantitative in situ correlation between microscopic MRI and polarized light microscopy studies of articular cartilage. Osteoarthritis Cartilage 2001;9:393–406, https://doi.org/10.1053/joca.2000.0405.
22. Lüsse S, Claassen H, Gehrke T, Hassenpflug J, Schünke M, Heller M, *et al*. Evaluation of water content by spatially resolved transverse relaxation times of human articular cartilage. Magn Reson Imaging 2000;18:423–30, https://doi.org/10.1016/S0730-725X(99)00144-7.
23. Wheaton AJ, Dodge GR, Elliott DM, Nicoll SB, Reddy R. Quantification of cartilage biomechanical and biochemical properties via T1rho magnetic resonance imaging. Magn Reson Med 2005;54:1087–93, https://doi.org/10.1002/mrm.20678.
24. Rautiainen J, Nissi MJ, Salo E-N, Tiitu V, Finnilä MAJ, Aho O-M, *et al*. Multiparametric MRI assessment of human articular cartilage degeneration: correlation with quantitative histology and mechanical properties. Magn Reson Med 2015;74:249–59, https://doi.org/10.1002/mrm.25401.
25. Berberat JE, Nissi MJ, Jurvelin JS, Nieminen MT. Assessment of interstitial water content of articular cartilage with T1 relaxation. Magn Reson Imaging 2009;27:727–32, https://doi.org/10.1016/j.mri.2008.09.005.
26. Xia Y, Wang N, Lee J, Badar F. Strain-dependent T1 relaxation profiles in articular cartilage by MRI at microscopic resolutions. Magn Reson Med 2011;65:1733–7, https://doi.org/10.1002/mrm.22933.
27. Nebelung S, Sondern B, Oehrl S, Tingart M, Rath B, Pufe T, *et al*. Functional MR imaging mapping of human articular cartilage response to loading. Radiology 2017;282:464–74, https://doi.org/10.1148/radiol.2016160053.
28. Nishii T, Kuroda K, Matsuoka Y, Sahara T, Yoshikawa H. Change in knee cartilage T2 in response to mechanical loading. J Magn Reson Imag 2008;28:175–80, https://doi.org/10.1002/jmri.21418.
29. Souza RB, Kumar D, Calixto N, Singh J, Schooler J, Subburaj K, *et al*. Response of knee cartilage T1rho and T2 relaxation times to in vivo mechanical loading in individuals with and without knee osteoarthritis. Osteoarthritis Cartilage 2014;22:1367–76, https://doi.org/10.1016/j.joca.2014.04.017.
30. Souza RB, Stehling C, Wyman BT, Hellio Le Graverand MP, Li X, Link TM, *et al*. The effects of acute loading on T1rho and T2 relaxation times of tibiofemoral articular cartilage. Osteoarthritis Cartilage 2010;18:1557–63, https://doi.org/10.1016/j.joca.2010.10.001.
31. Shepherd DE, Seedhom BB. Thickness of human articular cartilage in joints of the lower limb. Ann Rheum Dis 1999;58:27–34, https://doi.org/10.1136/ard.58.1.27.
32. Ahmed AM, Burke DL. In-vitro of measurement of static pressure distribution in synovial joints—Part I: tibial surface of the knee. J Biomech Eng 1983;105:216, https://doi.org/10.1115/1.3138409.
33. Epstein FH, Gilson WD. Displacement-encoded cardiac MRI using cosine and sine modulation to eliminate (CANSEL) artifact-generating echoes. Magn Reson Med 2004;52:774–81, https://doi.org/10.1002/mrm.20232.
34. Schneider CA, Rasband WS, Eliceiri KW. NIH Image to ImageJ: 25 years of image analysis. Nat Methods 2012;9:671–5, https://doi.org/10.1038/nmeth.2089.
35. Prince JL, Links JM. Medical Imaging Signals and Systems. 1st edn. New Jersey: Pearson Prentice Hall Upper Saddle River; 2006.
36. Nissi MJ, Rieppo J, Töyräs J, Laasanen MS, Kiviranta I, Jurvelin JS, *et al*. T2 relaxation time mapping reveals age- and species-related diversity of collagen network architecture in articular cartilage. Osteoarthritis Cartilage 2006;14:1265–71, https://doi.org/10.1016/j.joca.2006.06.002.
37. Goldstein RM, Zebker HA, Werner CL. Satellite radar interferometry: two-dimensional phase unwrapping. Radio Sci 1988;23:713–20, https://doi.org/10.1029/RS023i004p00713.
38. Geers MGD, De Borsts R, Brekelmans WAM. Computing strain fields from discrete displacement fields in 2D-solids. Int J Solid

Please cite this article in press as: Zevenbergen L, et al., Cartilage-on-cartilage contact: effect of compressive loading on tissue deformations and structural integrity of bovine articular cartilage, Osteoarthritis and Cartilage (2018), https://doi.org/10.1016/j.joca.2018.08.009

Struct 1996;33:4293–307, https://doi.org/10.1016/0020-7683(95)00240-5.
39. Park S, Ateshian GA. Dynamic response of immature bovine articular cartilage in tension and compression, and nonlinear viscoelastic modeling of the tensile response. J Biomech Eng 2006;128:623, https://doi.org/10.1115/1.2206201.
40. Akizuki S, Mow VC, Muller F, Pita JC, Howell DS, Manicourt DH. Tensile properties of human knee joint cartilage: I. Influence of ionic conditions, weight bearing, and fibrillation on the tensile modulus. J Orthop Res 1986;4:379–92, https://doi.org/10.1002/jor.1100040401.
41. Mow VC, Holmes MH, Michael Lai W. Fluid transport and mechanical properties of articular cartilage: a review. J Biomech 1984;17:377–94, https://doi.org/10.1016/0021-9290(84)90031-9.
42. Kääb MJ, Ito K, Clark JM, Nötzli HP. Deformation of articular cartilage collagen structure under static and cyclic loading. J Orthop Res 1998;16:743–51, https://doi.org/10.1002/jor.1100160617.
43. Kurkijärvi JE, Nissi MJ, Kiviranta I, Jurvelin JS, Nieminen MT. Delayed gadolinium-enhanced MRI of cartilage (dGEMRIC) and T2 characteristics of human knee articular cartilage: topographical variation and relationships to mechanical properties. Magn Reson Med 2004;52:41–6, https://doi.org/10.1002/mrm.20104.
44. Linka K, Itskov M, Truhn D, Nebelung S, Thüring J. T2 MR imaging vs. computational modeling of human articular cartilage tissue functionality. J Mech Behav Biomed Mater 2017;74:477–87, https://doi.org/10.1016/j.jmbbm.2017.07.023.
45. Williams GM, Klisch SM, Sah RL. Bioengineering cartilage growth, maturation, and form. Pediatr Res 2008;63:527–34, https://doi.org/10.1203/PDR.0b013e31816b4fe5.
46. Williamson AK, Chen AC, Masuda K, Thonar EJMA, Sah RL. Tensile mechanical properties of bovine articular cartilage: variations with growth and relationships to collagen network components. J Orthop Res 2003;21:872–80, https://doi.org/10.1016/S0736-0266(03)00030-5.
47. Williamson AK, Chen AC, Sah RL. Compressive properties and function - composition relationships of developing bovine articular cartilage. J Orthop Res 2001;19:1113–21, https://doi.org/10.1016/S0736-0266(01)00052-3.
48. Nissi MJ, Rieppo J, Töyräs J, Laasanen MS, Kiviranta I, Nieminen MT, *et al*. Estimation of mechanical properties of articular cartilage with MRI - dGEMRIC, T2 and T1 imaging in different species with variable stages of maturation. Osteoarthritis Cartilage 2007;15:1141–8, https://doi.org/10.1016/j.joca.2007.03.018.
49. Mosher TJ, Smith H, Dardzinski BJ, Schmithorst VJ, Smith MB. MR imaging and T2 mapping of femoral cartilage: in vivo determination of the magic angle effect. Am J Roentgenol 2001;177:665–9, https://doi.org/10.2214/ajr.177.3.1770665.
50. Vesanen PT, Zevenhoven KCJ, Nieminen JO, Dabek J, Parkkonen LT, Ilmoniemi RJ. Temperature dependence of relaxation times and temperature mapping in ultra-low-field MRI. J Magn Reson 2013;235:50–7, https://doi.org/10.1016/j.jmr.2013.07.009.

Please cite this article in press as: Zevenbergen L, et al., Cartilage-on-cartilage contact: effect of compressive loading on tissue deformations and structural integrity of bovine articular cartilage, Osteoarthritis and Cartilage (2018), https://doi.org/10.1016/j.joca.2018.08.009